Protein Sample Preparation

To isolate whole cellular protein extracts from cultured RPE cells, the cells were rinsed 3 times with 1× PBS (pH 7.4) and were lysed in a denaturing lysis buffer containing 7 M urea, 2 M thiourea, 4% CHAPS, 40 mM Tris, 0.2% purifier (Bio-Lyte, pH range 3–10; Bio-Rad, Hercules, CA), and 50 mM dithiothreitol (DTT). The collected lysate was then centrifuged at 14,000*g* for 15 minutes at 4°C. Proteins in the supernatant were repeatedly concentrated and precipitated and finally desalinated (Readyprep 2-D Cleanup kit; Bio-Rad). The protein concentration in the RPE samples was determined by a modified Lowry method adapted for use with the lysis buffer.

Two-Dimensional Electrophoresis

Protein samples were separated by a two-dimensional electrophoresis method. A 300-μg protein sample was loaded on immobilized pH gradient (IPG) strips (pH 3–10, 7 cm; pH 4–7, 17 cm; Bio-Rad) by in-gel rehydration at 20°C overnight. For the 7-cm strip, isoelectric focusing (IEF) was used for the first dimension at an initial voltage of 250 V for 15 minutes, increased to 4000 V for 2 hours, and held until 20,000 V/h was reached. For the 17-cm strip, the initial voltage was set at 250 V, as for the 7-cm strip. Then the voltage was increased to 10,000 V for 3 hours and was held until 60,000 V/h was reached. Immediately after IEF, the IPG strips were equilibrated for 20 minutes in buffer containing 6 M urea, 2% SDS, 0.375 M Tris (pH 8.8), and 20% glycerol under a reduced condition with 2% DTT (Bio-Rad), followed by another incubation for 10 minutes in the same buffer under alkylating conditions with 2.5% iodoacetamide (Bio-Rad).[15]

Equilibrated IPG strips were then electophoresed by SDS-PAGE for the second dimension. Images of the chemiluminescent signals were captured and merged with those of protein spots made visible by protein gel stain (Sypro Ruby; Bio-Rad), and the spots corresponding to the immunoreactivity were cut out. To test reproducibility, the experiment was performed twice.

Protein Identification by Mass Spectrometry

Excised gel pieces were rinsed with water and then with acetonitrile and were completely dried for the reduction-alkylation step. They were incubated with 10 mM DTT in 100 mM ammonium bicarbonate for 45 minutes at 56°C, then with 55 mM iodoacetamide in 100 mM ammonium bicarbonate for 30 minutes at room temperature in the dark. The supernatant was removed, and the washing procedure was repeated three times. Finally, the gel pieces were again completely dried before trypsin digestion and were rehydrated in a solution of trypsin (12.5 ng/μL; Promega, Madison, WI) in 50 mM ammonium bicarbonate. The digestion was continued for 16 hours at 37°C, and the extraction step was performed once with 25 mM ammonium bicarbonate, then twice with 5% formic acid, and finally with water. After resuspension in 40 μL solution of aqueous 0.1% trifluoroacetic acid/2% acetonitrile, the samples were analyzed by liquid chromatography coupled to tandem mass spectrometry (LC-MS/MS). For analysis by LC-MS/MS, the tryptic digests were injected by an automatic sampler (HTS-PAL, CTC Analytics, Zwingen, Switzerland) onto a 0.2 × 50-mm capillary reversed-phase column (Magic C18, 3 μm; Michrom BioResources, Inc., Auburn, CA) using an HPLC (Paradigm MS4; Michrom BioResources). Peptides were eluted with a gradient (95% solvent A consisting of 98% H_2O/2% acetonitrile/0.1% formic acid)/5% solvent B (10% H_2O/90% acetonitrile/0.1% formic acid; 0 minute)/35% solvent A/65% solvent B (20 minutes)/5% solvent A/95% solvent B (21 minutes)/5% solvent A/95% solvent B (23 minutes)/95% solvent A/5% solvent B (30 minutes) for 30 minutes at a flow rate of 1.5 μL/min. Peptides were eluted directly into an ion trap mass spectrometer (ESI; Finnigan LTQ; Thermo Electron Corporation, Waltham, MA) capable of data-dependent acquisition. Each full MS scan was followed by an MS/MS scan of the most intense peak in the full MS spectrum with the dynamic exclusion enabled to allow detection of less-abundant peptide ions. Mass spectrometric scan events and HPLC solvent gradients were controlled with the use of a computer program (Paradigm Home; Michrom BioResources).

Total RNA Isolation from RPE Cells

Total RNA was isolated from the cultured RPE cells after 6 hours, 12 hours, and 24 hours with TFPI-2 using a total RNA isolation kit (RNA-Bee-RNA Isolation Reagent; Tel-Test, Friendswood, TX). Total RNA samples were treated with RNase-free DNase (Roche Diagnostics Japan) to minimize genomic DNA contamination.

DNA Microarray Analysis

DNA microarray analysis was performed (AB1700 Chemiluminescent Microarray Analyzer; Applied Biosystems, Foster City, CA). The survey array used (Human Genome Survey Array; Applied Biosystems) contained 33,096 60-mer oligonucleotide probes representing a set of 27,868 individual human genes and more than 1000 control probes. Sequences used for the microarray probe were obtained from curated transcripts (Celera Genomics Human Genome Database), RefSeq transcripts that had been structurally curated from the LocusLink public database, high-quality cDNA sequences from the Mammalian Gene Collection (MGC; http://mgc.nci.nih.gov), and transcripts that were experimentally validated (Applied Biosystems). The 60-mer oligo probes were synthesized using standard phosphoramidite chemistry and solid-phase synthesis and underwent quality control by mass spectrometry. The probes were deposited and covalently bound to a derivatized nylon substrate (2.5 × 3 inches) that was backed by a glass slide by contact spotting with a feature diameter of 180 μm and more than 45 μm between each feature. A 24-mer oligo internal control probe (ICP) was cospotted at every feature with 60-mer gene expression probe on the microarray. Digoxigenin-UTP labeled cRNA was generated and linearly amplified from 1 μg total RNA (Chemiluminescent RT-IVT Labeling Kit, version 2.0; Applied Biosystems) according to the manufacturer's protocol. Array hybridization (two arrays per sample), chemiluminescence detection, image acquisition, and analysis were performed (Chemiluminescence Detection Kit and AB1700 Chemiluminescent Microarray Analyzer; Applied Biosystems) according to the manufacturer's protocol.

Briefly, each microarray was first prehybridized at 55°C for 1 hour in hybridization buffer with blocking reagent. Sixteen micrograms labeled cRNA targets were first fragmented into 100 to 400 bases by incubation with fragmentation buffer at 60°C for 30 minutes, mixed with internal control target (ICT; 24-mer oligo labeled with LIZR fluorescent dye), and hybridized to each prehybrid microarray in 1.5 mL vol at 55°C for 16 hours. After hybridization, the arrays were washed with hybridization wash buffer and chemiluminescence rinse buffer. Enhanced chemiluminescent signals were generated by first incubating the arrays with anti–digoxigenin alkaline phosphatase and enhanced with chemiluminescence enhancing solution and chemiluminescence substrate.

Images were collected from each microarray using the 1700 analyzer equipped with a high-resolution, large-format CCD camera, including 2 "short" chemiluminescent images (5-second exposure length each) and 2 "long" chemiluminescent images (25-second exposure length each) for gene expression analysis, two fluorescent images for feature finding and spot normalization, and two quality control images for spectrum cross-talk correction. Images were quantified, corrected for background and spot, and spatially normalized.

Data Analysis

MS data were identified with the use of a protein search program (BioWorks 3.2; Thermo Electron Corporation, Waltham, MA). For protein database searches, the same program was used to create centroid peak lists from the raw spectra. These peak lists were then submitted for database searching (BioWorks). The identity of the samples was searched from databases (nrNCBI [www.ncbi.nlm.nih.gov]) that extracted proteins and were restructured; search terms included human and *Homo sapiens*. Differentially expressed proteins were further analyzed for related genes and proteins using natural language processing software (Pubgene database; PubGene Inc., Boston, MA) and data mining software of gene expression (OmniViz; OmniViz, Inc., Maynard, MA).

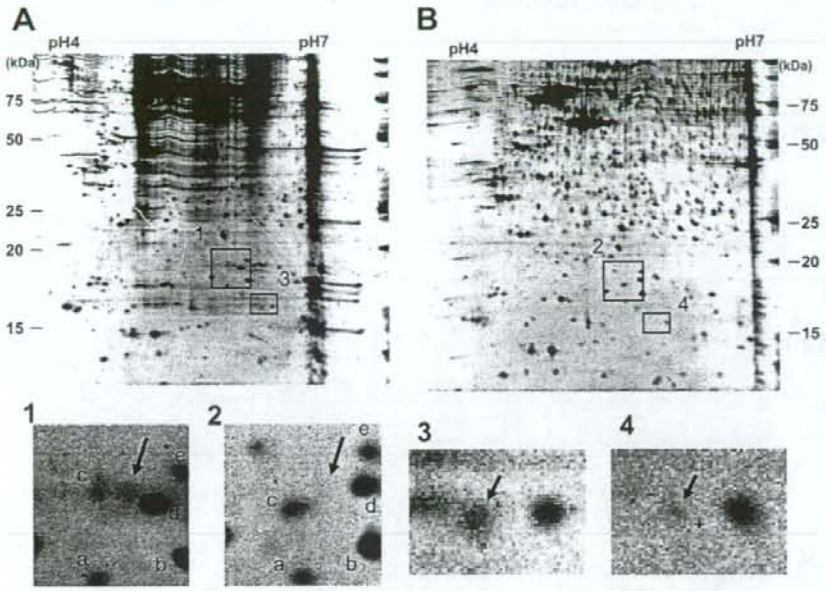

FIGURE 1. Two-dimensional gel electrophoresis of human RPE cells culture with (A) and without (B) TFPI-2. Spots corresponding to proteins whose expression is dependent on the presence of TFPI-2 in the culture medium are indicated by the *arrows* (*insets*). Proteins were detected by SYPRO Ruby staining. Spots corresponding to the differentially expressed proteins indicated by *arrows* (1 vs. 2 and 3 vs. 4) were subsequently subject to the LC-MS/MS analysis so that proteins could be identified.

RESULTS

Proteome Analysis of RPE Cells Treated with TFPI-2

To determine the mechanisms responsible for the proliferation-promoting activity of TFPI-2 on RPE cells, protein synthesis and RNA expression were determined before and after TFPI-2 exposure. Differentially expressed proteins in the primary human RPE cells in response to TFPI-2 were identified by two-dimensional electrophoresis (Fig. 1). Samples were initially separated using IPG at a pH range of 3 to 10 to observe the full distribution of protein spots. The pH range was then narrowed to 4 to 7 to obtain higher resolution for spot picking. Consequently, approximately 480 spots were identified in the whole gel. We then focused on molecular weight less than 25 kDa, which is easy to check for changes. Ten spots considered differentially expressed in the two-dimensional gel were collected and subjected to LC-MS/MS analysis. Among the identified proteins, ribosomal protein L11 (RPL11; Fig. 1-1) and c-Myc binding protein (MYCBP; Fig. 1-3), known for regulating cell proliferation, were identified.[16] These two proteins, identified by LC-MS/MS analysis and data analysis software (Bioworks 3.2), were consistent with those estimated from the results of two-dimensional electrophoresis (Table 1).

Transcriptomic Analysis of RPE Cells Treated with TFPI-2

The expression of 8134 genes in RPE cells was analyzed using DNA microarray with and without TFPI-2 exposure for 6 hours, 12 hours, and 24 hours. Signal normalization was performed for six independent DNA microarray chips according to the manufacturer's protocol. Genes differentially expressed by more than threefold were considered significant and were selected for further analysis. Among the 33,096 possible probes, 10,773 probes were detected in the RPE cells incubated with TFPI-2, whereas only 2186 probes were detected without TFPI-2. Based on expression levels at the three time points (6 hours, 12 hours, and 24 hours), the time-dependent expression pattern of each gene was calculated and clustered with other genes with similar expression patterns using data mining software (OmniViz). Data analysis resulted in 38 clusters of genes that either increased or decreased their expression levels by more than twofold after TFPI-2 (Fig. 2). Nineteen genes were upregulated in 5 clusters, 108 genes in 16 clusters, and 717 genes in 22 clusters at 6 hours, 12 hours, and 24 hours, respectively. For downregulated genes, 30 genes in 16 clusters, 119 genes in 19 clusters, and 3 genes in 19 clusters were observed after 6 hours, 12 hours, and 24 hours, respectively. Transcriptomic analysis revealed significantly more genes differentially expressed at the transcriptional level than at the proteome level.

DISCUSSION

Proteins and genes whose expression was upregulated or downregulated after exposure to TFPI-2 were analyzed in human RPE cells to study the proteomic and transcriptomic changes. Protein and gene expression profiles for human RPE cells have been reported by West et al.,[17] who identified 278 proteins, and Cai et al.,[18] who reported 5580 ± 84 genes expressed in adult human RPE and ARPE19 cell lines using a DNA chip with 12,600 probes (Human U95Av2; Affymetrix, Santa Clara, CA). Our study showed changes in the expression of 8134 of 27,868 genes. DNA microarray analyses were simul-

TABLE 1. Two-Dimensional Gel Spots Identified by Mass Spectrometry

Protein	Number of AA	Peptide Residues	Identified Peptide from Database	MW	Score	Accession Number
c-Myc binding protein	167	108–117	TAEDAKDFFK	18642.6	10.13	1731809
Ribosomal protein L11	177	88–94	VREYELR	20125.1	20.21	14719845

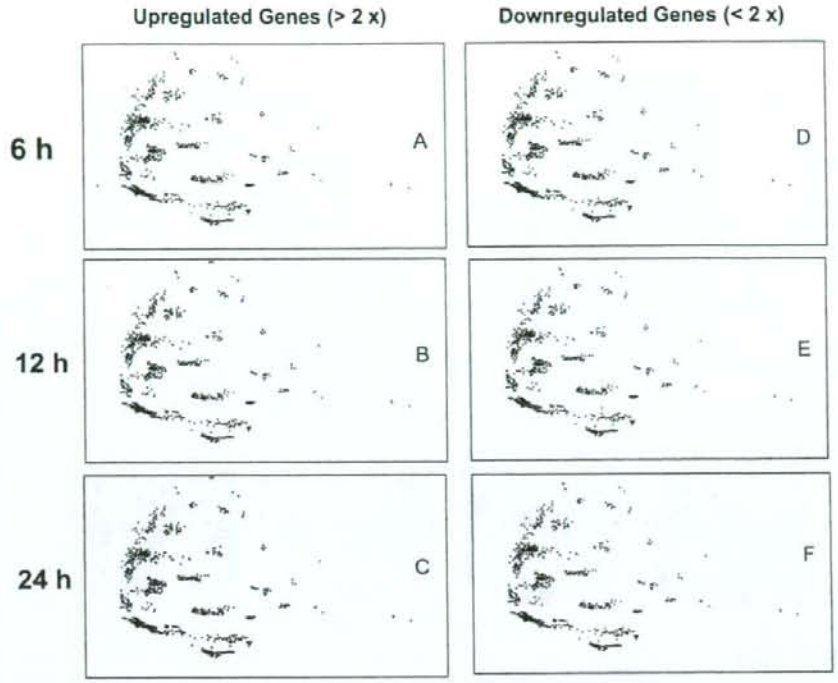

FIGURE 2. Differentially expressed genes detected by DNA array are plotted as clusters. Differentially expressed genes whose expression level was increased by more than twofold (**A**–**C**) or was reduced by more than 0.5-fold (**D**–**F**) in RPE cells treated with TFPI-2 at incubation times of 6 hours, 12 hours, and 24 hours compared with the control cells are shown. Expression profile analysis revealed different gene expression patterns at each incubation time.

taneously performed at three time points (6 hours, 12 hours, and 24 hours) to monitor the course of expression of the possible 27,868 genes in human RPE cells exposed and not exposed to TFPI-2. This study was conducted at the translational and the transcriptional levels to complement the disadvantages of each method.

Raw gene expression data were further analyzed with data mining software (OmniViz) to obtain an overall picture of the transcriptional changes induced by TFPI-2 in human primary RPE cells. Genes whose expressions were changed by more than twofold were clustered into 38 groups showing a change of expression at each time point (Fig. 2). The number of genes upregulated at each time point was considerably higher than the number that was downregulated. A small number of genes was triggered by TFPI-2 treatment at 6 hours, before the major changes occurred at 24 hours. Among the initially upregulated genes were reticulon 4 interacting protein 1, phospholipase C, delta 1, granzyme M (lymphocyte met-ase 1; *GZMM*), and mitochondrial ribosomal protein L41 (*MRPL41*).

Proteomics analysis simultaneously performed at 24 hours identified two differentially expressed proteins, the c-*myc* binding protein (MYCBP) and the ribosomal protein L11 (RPL11). MYCBP and RPL11 (Fig. 3) are well known to regulate cell cycling through the Rb/E2F pathway and the p53 pathway, respectively. MYCBP stimulates c-*myc* transcription through the retinoblastoma protein (Rb)/E2F pathway (see Fig. 5). Sears et al.[19] reported that activation of Myc increased the signal transduction of the cyclin D/cdk4 and cyclin E/cdk2 pathways. Activation of these pathways inactivates Rb after phosphorylation and E2F dissociation, which then promotes RPE cells to go into the S-phase of the cell cycle. The twofold transcriptional increase of *Rb* and *E2F3* in TFPI-2 exposed cells compared with control at 24 hours supports this hypothesis (Figs. 4C, 4F).

Concomitantly, the expressions of Rb and Mdm2 were upregulated twofold in growth-stimulated cells compared with control cells. Because Rb is associated with the negative regulation of the G_1-phase of the cell cycle, the enhanced expres-

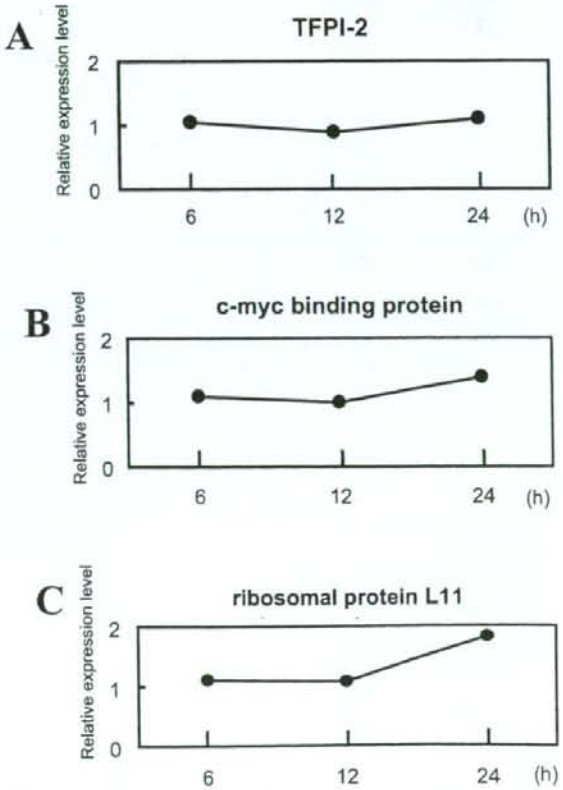

FIGURE 3. Time course of gene expression for TFPI-2 (**A**), c-*myc* binding protein (**B**), and ribosomal protein L11 (**C**) in the cultured human RPE cells after exposure to TFPI-2.

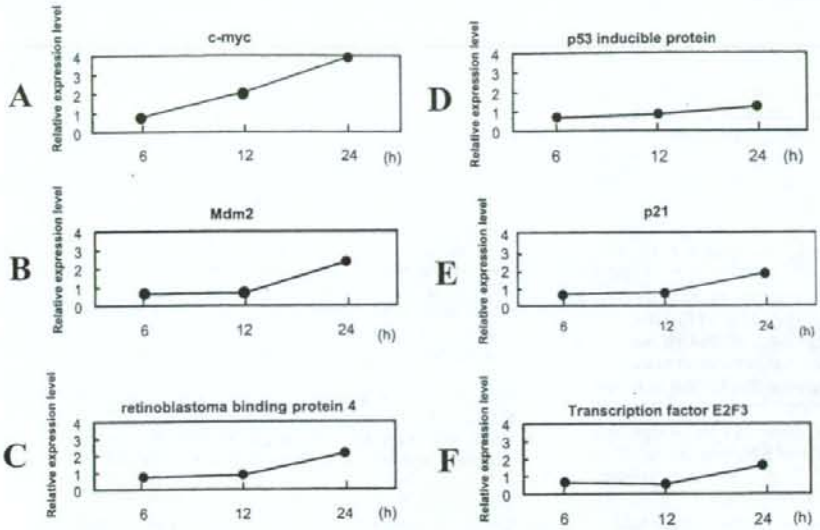

FIGURE 4. Time courses of protein expression patterns for c-*myc* (**A**), Mdm2 (**B**), retinoblastoma binding protein 4 (**C**), p-53 inducible protein (**D**), p21 (**E**), and transcription factor E2F3 in the cultured human RPE cells after exposure to TFPI-2.

sion of *Mdm2* might have been involved in the augmented degradation of Rb through the ubiquitin/proteasome-dependent pathway. Recently, Uchida et al.[20] suggested that Mdm2 regulates the function of RB through the ubiquitin-dependent degradation of RB.

The *Rb* gene was the first identified tumor-suppressor gene,[21] and it was recognized as a central component of a signaling pathway that controlled cell proliferation. Specifically, the D-type G_1 cyclins, together with their associated cyclin-dependent kinases (CKDs) Cdk4 and Cdk6, initiated the phosphorylation of Rb and Rb family members, inactivating their capacity to interact with the E2F transcription factors (Fig. 5).[19] This phosphorylation leads to an accumulation of E2F1, E2F2, and E2F3a, which activate the transcription of a large number of genes essential for DNA replication and further cell cycle progression.[22–26] Among the E2F targets are genes encoding a second class of G_1 cyclins, cyclin E, and the associated kinase Cdk2 (Fig. 5).[19] The activation of cyclin E/Cdk2 kinase activity by E2F leads to further phosphorylation and inactivation of Rb, further enhancing E2F activity and increasing the accumulation of cyclin E/Cdk2 (Fig. 5).[19] This feedback loop, which leads to a continual inactivation of *Rb* independent of the action of cyclin D/Cdk4—defined as a junction in cell proliferation response when passaged through the cell cycle—becomes growth factor independent.[25,26] The activity of the G_1 Cdks is negatively regulated by a family of cyclin-dependent kinase inhibitors (CKIs), including $p21^{WAF1}$, $p27^{Kip1}$, and the $p16^{INK4a}$ family.[27] The three upregulated E2Fs associate exclusively with Rb and appear to play a positive role in cell cycle progression.[19]

RPL11 binds the mouse double-minute 2 (Mdm2 is the mouse homologue of Hdm2 in humans) protein with other ribosomal proteins (L23 and L5) to form a complex to inhibit ubiquitin-dependent degradation of p53.[28–30] The RPL11 protein is expressed in ARPE-19 cells.[31] Inhibition of p53 degradation leads to p21 signaling, which participates in the G_1

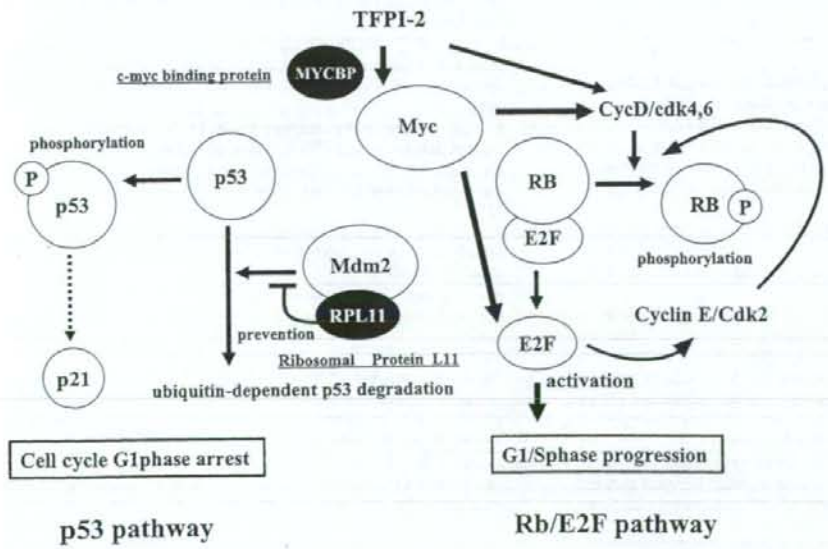

FIGURE 5. Hypothetical network of various genes and proteins associated with the growth-promoting effect of TFPI-2 on the human RPE cells. *Arrows*: stimulatory signals. *Straight* and *dotted lines*: inhibitory effects.

arrest of the cell cycle but also negatively regulates cell proliferation (Fig. 5).[30,32–34] In support of this hypothesis, *p21* transcription was increased by twofold after 24 hours by TFPI-2.

The *p53* gene mediates a major tumor-suppression pathway in mammalian cells and is frequently altered in human tumors.[30] Its function is kept at a low level during normal cell growth and is activated in response to various cellular stresses by acting as a sequence-specific transcription factor.[30] The p53 protein induces cell cycle arrest or apoptosis.[30]

Shinoda et al.[14] reported cell growth proliferation of vascular smooth muscle endothelial cells by a purified mitogenic substance from human umbilical vein endothelial cells, later identified as TFPI-2. These authors showed the rapid activation of mitogen-activated protein kinase (MAPK) by TFPI-2 and the induced activation of proto-oncogene *c-fos* mRNA in smooth muscle cells.[14] They concluded that *c-fos* activation was initiated by MAPK based on MAPK inhibitor PD098059 suppression.

In conclusion, the results of proteomic and transcriptomic analyses suggest that the proliferation of RPE cells induced by TFPI-2 is regulated through the Rb/E2F, p53, and Ras/Raf/MAPK pathways. We and others[3,35] have reported a transcript of TFPI-2 in the mRNA of RPE cells. It is now reasonable to expect that RPE cells are able to self-proliferate by generating TFPI-2. Additional studies are needed to determine whether TFPI-2 can act as such an autocrine factor and can be modified for future treatment of the dry-type age-related macular degeneration and of retinitis pigmentosa.

References

1. Hughes BA, Gallemore RP, Miller SS. Transport mechanisms in the retinal pigment epithelium. In: Marmor MF, Wolfensberger TJ, eds. *The Retinal Pigment Epithelium: Function and Disease*. New York: Oxford University Press; 1998:103–134.
2. Haruta M. Embryonic stem cells: potential source for ocular repair. *Semin Ophthalmol*. 2005;20:17–23.
3. Tanaka Y, Utsumi J, Matsui M, et al. Purification, molecular cloning, and expression of a novel growth-promoting factor for retinal pigment epithelial cells, REF-1/TFPI-2. *Invest Ophthalmol Vis Sci*. 2004;45:245–252.
4. Chand HS, Foster DC, Kisiel W. Structure, function and biology of tissue factor pathway inhibitor-2. *Thromb Haemost*. 2005;94:1122–1130.
5. Schmidt AE, Chand HS, Cascio D, et al. Crystal structure of Kunitz domain 1 (KD1) of tissue factor pathway inhibitor-2 in complex with trypsin: implications for KD1 specificity of inhibition. *J Biol Chem*. 2005;280:27832–27838.
6. Chand HS, Schmidt AE, Bajaj SP, et al. Structure-function analysis of the reactive site in the first Kunitz-type domain of human tissue factor pathway inhibitor-2. *J Biol Chem*. 2004;279:17500–17507.
7. Sprecher CA, Kisiel W, Mathewes S, et al. Molecular cloning, expression, and partial characterization of a second human tissue-factor-pathway inhibitor. *Proc Natl Acad Sci USA*. 1994;91:3353–3357.
8. Yanamandra N, Kondraganti S, Gondi CS, et al. Recombinant adeno-associated virus (rAAV) expressing TFPI-2 inhibits invasion, angiogenesis and tumor growth in a human glioblastoma cell line. *Int J Cancer*. 2005;115:998–1005.
9. Rollin J, Iochmann S, Blechet C, et al. Expression and methylation status of tissue factor pathway inhibitor-2 gene in non-small-cell lung cancer. *Br J Cancer*. 2005;92:775–783.
10. Konduri SD, Srivenugopal KS, Yanamandra N. Promoter methylation and silencing of the tissue factor pathway inhibitor-2 (TFPI-2), a gene encoding an inhibitor of matrix metalloproteinases in human glioma cells. *Oncogene*. 2003;22:4509–4516.
11. Santin AD, Zhan F, Bignotti E, et al. Gene expression profiles of primary HPV16- and HPV18-infected early stage cervical cancers and normal cervical epithelium: identification of novel candidate molecular markers for cervical cancer diagnosis and therapy. *Virology*. 2005;331:269–291.
12. Sato N, Parker AR, Fukushima N, et al. Epigenetic inactivation of TFPI-2 as a common mechanism associated with growth and invasion of pancreatic ductal adenocarcinoma. *Oncogene*. 2005;24:850–858.
13. Kast C, Wang M, Whiteway M. The ERK/MAPK pathway regulates the activity of the human tissue factor pathway inhibitor-2 promoter. *J Biol Chem*. 2003;278:6787–6794.
14. Shinoda E, Yui Y, Hattori R, et al. Tissue factor pathway inhibitor-2 is a novel mitogen for vascular smooth muscle cells. *J Biol Chem*. 1999;274:5379–5384.
15. Bahk SC, Lee SH, Jang JU, et al. Identification of crystallin family proteins in vitreous body in rat endotoxin-induced uveitis: involvement of crystallin truncation in uveitis pathogenesis. *Proteomics*. 2006;6:3436–3444.
16. Taira T, Maëda J, Onishi T, et al. AMY-1, a novel C-MYC binding protein that stimulates transcription activity of C-MYC. *Genes Cells*. 1998;3:549–565.
17. West KA, Yan L, Shadrach K, et al. Protein database, human retinal pigment epithelium. *Mol Cell Proteomics*. 2003;2:37–49.
18. Cai H, Del Priore LV. Gene expression profile of cultured adult compared to immortalized human RPE. *Mol Vis*. 2006;12:1–14.
19. Sears RC, Nevins JR. Signaling networks that link cell proliferation and cell fate. *J Biol Chem*. 2002;277:11617–11620.
20. Uchida C, Miwa S, Kitagawa K, et al. Enhanced Mdm2 activity inhibits pRB function via ubiquitin-dependent degradation. *EMBO J*. 2005;24:160–169.
21. Hanahan D, Weinberg RA. The hallmarks of cancer. *Cell*. 2000;100:57–70.
22. Dyson N. The regulation of E2F by pRB-family proteins. *Genes Dev*. 1998;12:2245–2262.
23. Nevins JR. Toward an understanding of the functional complexity of the E2F and retinoblastoma families. *Cell Growth Differ*. 1998;9:585–593.
24. Harbour JW, Dean DC. Rb function in cell-cycle regulation and apoptosis. *Nat Cell Biol*. 2000;2:E65–E67.
25. Dou QP, Levin AH, Zhao S, Pardee AB. Cyclin E and cyclin A as candidates for the restriction point protein. *Cancer Res*. 1993;53:1493–1497.
26. Pardee AB. A restriction point for control of normal animal cell proliferation. *Proc Natl Acad Sci USA*. 1974;71:1286–1290.
27. Sherr CJ, Roberts JM. CDK inhibitors: positive and negative regulators of G1-phase progression. *Genes Dev*. 1999;13:1501–1512.
28. Krystof V, McNae IW, Walkinshaw MD. Antiproliferative activity of olomoucine II, a novel 2,6,9-trisubstituted purine cyclin-dependent kinase inhibitor. *Cell Mol Life Sci*. 2005;62:1763–1771.
29. Dai MS, Lu H. Inhibition of MDM2-mediated p53 ubiquitination and degradation by ribosomal protein L5. *J Biol Chem*. 2004;279:44475–44482.
30. Zhang Y, Wolf GW, Bhat K, et al. Ribosomal protein L11 negatively regulates oncoprotein MDM2 and mediates a p53-dependent ribosomal-stress checkpoint pathway. *Mol Cell Biol*. 2003;23:8902–8912.
31. Rao KC, Palamalai V, Dunlevy JR, et al. Peptidyl-Lys metalloendopeptidase-catalyzed ^{18}O labeling for comparative proteomics: application to cytokine/lipolysaccharide-treated human retinal pigment epithelium cell line. *Mol Cell Proteomics*. 2005;4:1550–1557.
32. Chao C, Saito S, Kang J. p53 transcriptional activity is essential for p53-dependent apoptosis following DNA damage. *EMBO J*. 2000;19:4967–4975.
33. Bai F, Matsui T, Ohtani-Fujita N, et al. Promoter activation and following induction of the p21/WAF1 gene by flavone is involved in G1 phase arrest in A549 lung adenocarcinoma cells. *FEBS Lett*. 1998;437:61–64.
34. Nyunoya T, Powers LS, Yarovinsky TO. Hyperoxia induces macrophage cell cycle arrest by adhesion-dependent induction of p21Cip1 and activation of the retinoblastoma protein. *J Biol Chem*. 2003;278:36099–360106.
35. Ortego J, Escribano J, Coca-Prados M. Gene expression of protease and protease inhibitors in the human ciliary epithelium and ODM-2 cells. *Exp Eye Res*. 1997;65:289–299.

Source Book of Models for Biomedical Research

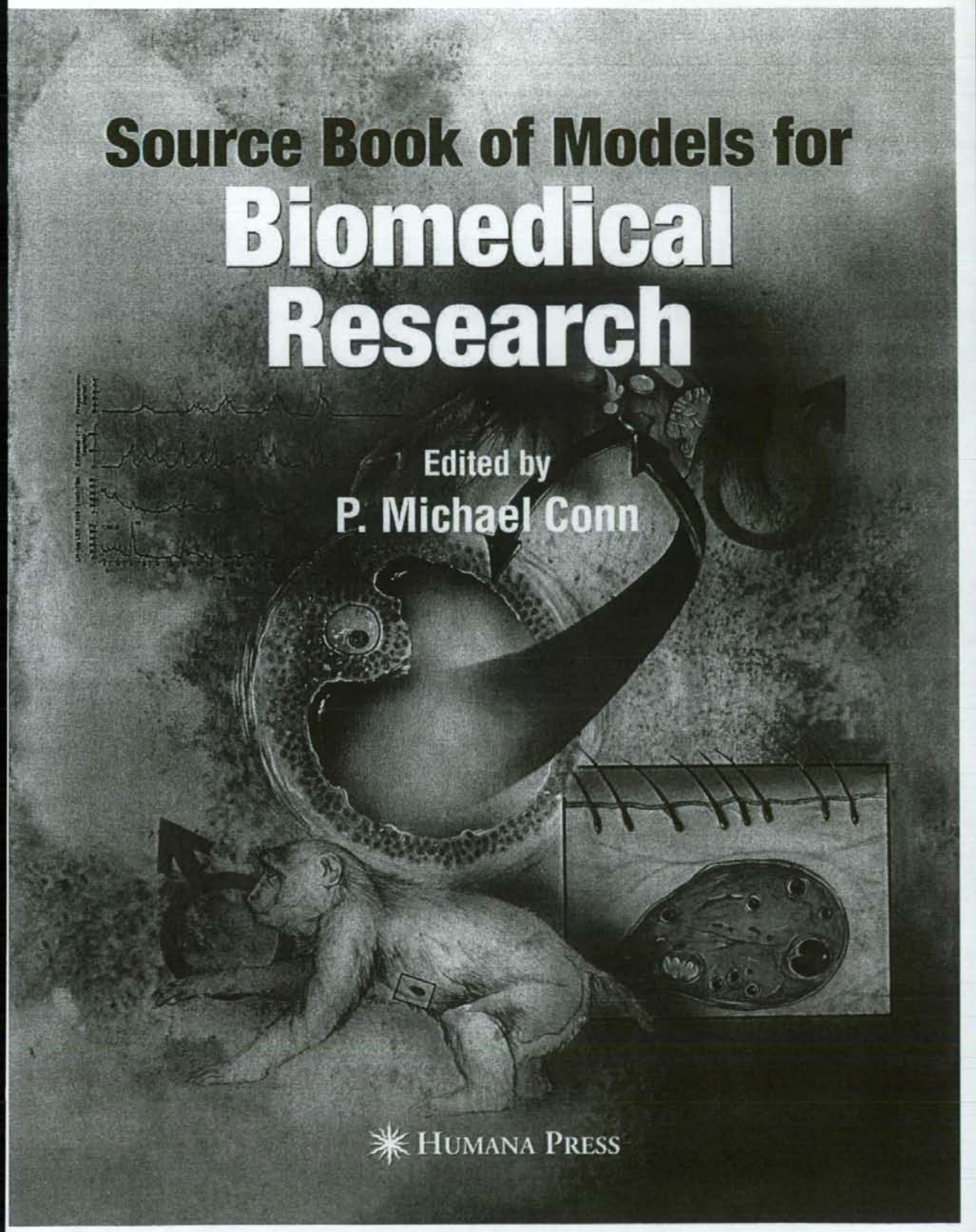

Edited by

P. Michael Conn

HUMANA PRESS

Source Book of Models for Biomedical Research

Chapter 33: Animal Models for Eye Diseases and Therapeutics

Subtitle: Animal models of Age-Related Macula Degeneration and glaucoma

Takeshi Iwata, Ph.D.[1] and Stanislav Tomarev, Ph.D.[2]

[1]National Institute of Sensory Organs, National Hospital Organization Tokyo Medical Center, 2-5-2 Higashigaoka, Meguro-ku, Tokyo 152-8902 Japan.

TEL/FAX: +81-(3)3411-1026

e-mail: iwatatakeshi@kankakuki.go.jp

[2]National Eye Institute, National Institutes of Health, Bldg. 7, Rm. 103, 7 Memorial Drive, MSC 0704, Bethesda, MD 20892-0704 USA.

TEL: (301)496-8524

FAX: (301)496-8760

e-mail: tomarevs@nei.nih.gov

***Key Words**: Vision, Age-related macular degeneration, Retina, Macula, Drusen, Glaucoma, Retinal ganglion cells, Optic nerve*

1. Visual impairment and importance of animal models for eye diseases

It is believed that more than 80% of the information our brain receives comes from the visual system. Dysfunction of the visual system can alter the normal human life style and significantly lower the quality of life. The causes of visual impairments and blindness vary among ethnic groups and the global regions where they live. There are many causes of visual impairments including diabetic complications, infections, and trauma, however the most prevalent causes of visual impairment are cataracts, glaucoma, and age-related macular degeneration (AMD). According to the World Health Organization, there were more than 161 million visually impaired individuals in 2002, and 124 million of this group had low vision and 37 million were blind (http://www.who.int/mediacentre/factsheets/fs282/en/index.html) (Fig. 1).

Cataract, glaucoma, and AMD are responsible for 69% of blindness globally. Although cataracts are the leading cause of blindness worldwide, recent advances in cataract surgery has significantly reduced the visual impairments caused by cataracts especially in developed countries. Glaucoma, an optic neuropathy, is often associated with elevated intraocular pressure and is responsible for blindness in 6.7 million people

across the world. Glaucoma is more common in individuals of African ancestry, and the incidence of glaucoma increases with age.

The most prevalent eye disease for elderly Europeans and Americans is AMD. This degenerative disease progresses from retinal deposits called drusen to neovascularization and retinal hemorrhages resulting in irreversible loss of central vision.

In spite of the high incidence of AMD and glaucoma, a limited amount of information is available on the underlying pathological mechanisms causing these diseases. Obtaining tissues for any disease is often difficult, and even when obtained, they may not be informative because the tissues are usually collected many hours or even days after death. Because experimental studies of AMD and glaucoma are limited in humans, the availability of animal models is very valuable because they can be used to investigate the molecular mechanisms causing these diseases and to test new therapeutic interventions. Animal models, compared to other experimental methods, e.g., cell and organ cultures or postmortem models, allow the study of different pathological factors and therapeutical treatments under in vivo conditions, i.e., with the visual and other systems of the body intact. Appropriate animal models, e.g., monkey,

mouse, zebrafish, also facilitate the identification of new genes involved in the pathology as well as elucidate the genetic relationships between causative and modifier genes. Equally important, specific genes can be altered in these models. Thus, it is possible to induce mutations in animals, and then search for specific phenotypes, e.g., abnormal intraocular pressure (IOP) and retinal ganglion cell degeneration. Subsequently, the affected genes can be identified by standard genetic procedures.

Many animal models of AMD and glaucoma have been developed in different mammalian and non-mammalian species. None of these models is a perfect reproduction of the human disease, and when choosing the animal model for research, the investigator should evaluate the following: 1) similarity of the visual system of the model to that of humans especially the eye; 2) similarity of the time course of pathological changes in the model and in human eyes; 3) ability to perform genetic manipulations; 4) training required to produce affected animals; 5) size of the eye; 6) availability and difficulties in the methods of analysis; 7) availability of animals; and 8) cost.

2. Age-related macular degeneration (AMD)

2.1. Introduction of AMD

The retina is composed of nine layers of neural and glial cells that are arranged concentrically at the posterior pole of the eye. Incoming light is focused on the central area of the retina called the fovea which is located in the center of the macular area (Fig. 2). In humans, the size of the macula is approximately 6 mm in diameter (Fig.3). The outer (posterior) surface of the retina is covered by a monolayer of retinal pigment epithelial (RPE) cells which forms a diffusion barrier between the neural retina and the choroidal blood supply. The RPE regulates the transport of proteins to the retina, and controls the hydration and ionic composition of the subretinal space. The physiological condition of the RPE is closely associated with the pathogenesis of AMD.

AMD is a blinding disorder characterized by a marked decrease in central vision associated with RPE atrophy with or without choroidal neovascularization (CNV). Many factors including genetic, behavioral, and environmental, are involved in this disease. AMD is characterized by the degeneration of cone photoreceptors in the foveal region of the retina resulting in a decrease of central visual acuity. The progressive impairment of

the retinal pigment epithelial (RPE) cells, and damage to Bruch's membrane and choriocapillaris results in retinal atrophy and photoreceptor dysfunction. In some cases, CNV develops, and the new vessels penetrate Bruch's membrane and pass into the subretinal space.

Two types of AMD are recognized; the non-neovascular type is called the dry-type AMD and includes more than 80% of the cases, and the neovascular type is called the wet-type AMD which is progressive with a higher probability of blindness. The prevalence of AMD differs considerably among the different ethnic groups, but the incidence increases with age in all groups. A lower prevalence of AMD has been reported in individuals of African ancestry than of Anglo-Saxon ancestry. Other risk factors for AMD are cigarette smoking, obesity, hypertension, and atherosclerosis.

2.2. Epidemiology and genetics of AMD

Extensive epidemiological studies have shown a genetic component for AMD. Thus, twin studies have shown a higher concordance for AMD in monozygotic twins than in dizygotic twins (1-3). In addition, first degree relatives of individuals with AMD

have a 2 to 4 fold higher incidence of AMD over individuals without a family history of AMD. Genetic segregation studies have also shown a genetic effect that accounts for approximately 60% of AMD with a single major gene accounting for about 55% of the risk of developing AMD. Overall, the data have suggested that the etiology of AMD has a significant genetic component. Only a small proportion of the families with AMD show Mendelian inheritance, and the majority of the individuals inherit AMD in a complex multi-gene pattern.

There have been a number of attempts to identify the genes which cause AMD. With the help of the haplotype marker project (HapMap Project), genome wide scanning has identified at least 13 loci linked to AMD on different chromosomes (4-6).

Recently, a polymorphism of complement factor H gene (*Y402H*) was shown to be associated with an increased risk for AMD (7-10). These results were confirmed in many of the countries with large Caucasian populations but not in Japan (11,12). This gene is located on chromosome 1q25-31 where one of the candidate loci was identified by linkage studies. Another recent study reported that a haplotype association of tandemly located complement 2 and factor B was protective for AMD (13).

2.3. Pathology and biochemistry of AMD

The early stage of the dry type AMD is characterized by a thickening of Bruch's membrane, aggregation of pigment granules, and increasing numbers of drusen. The thickening of Bruch's membrane obstructs its function as a 'barrier' between the choroid and the RPE that protects the neural retina from the choriocapillary. Drusen are small yellowish-white deposits that are composed of lipids, proteins, glycoproteins, and glycosaminoglycans. They accumulate in the extracellular space and the inner aspects of Bruch's membrane (Fig. 3). Drusen are not directly associated with visual loss but represent a risk factor for both the dry-type and wet-type AMD. The classification of hard and soft drusen is based on their size, shape, and color; hard drusen are yellowish with diameters <50 μm and are found in eyes that are less likely to progress to advanced stages of the disease, while soft drusen are darker yellow and larger in size, and are found in eyes more likely to progress to more advanced stages of AMD. A small percentage of dry-type AMD patients progress to the late stage of the wet-type AMD that is characterized by geographic atrophy or detachment of RPE and the

development of CNV in the macular region. The presence of a CNV is the factor that most damages the neural retina because the newly developed vessels grow from the choriocapillaris through Bruch's membrane and extend laterally through the RPE cell layer (classic CNV) or extend between the inner Bruch's membrane and RPE (occult CNV). In advanced stages of AMD, the CNV and fluid leaked into the subretinal or intraretinal regions leads to cell death and retinal detachment.

Recent analyses of the progression of drusen have provided important clues that help understand the molecular pathology of AMD. Using both immunohistochemistry and proteomic techniques, the materials in drusen were found to be composed of molecules that mediate inflammatory and immune processes (14, 15). These molecules include components of the complement pathway and modulators of complement activation, viz., vitronectin, clusterin, membrane cofactor protein, and complement receptor-1. In addition, molecules triggering inflammation, viz., amyloid P component, a1-antitrypsin, and apolipoprotein E, were identified in drusen. Cellular debris from macrophages, RPE cells, and choroidal dendritic cells has also been identified in drusen. On the other hand, crystallins, EEFMP1, and amyloid-beta have been found at

higher levels in drusen from individuals unaffected by AMD. The presence of immunoreactive proteins and the oxidative modifications of many proteins in drusen imply that both oxidation and immune functions are involved in the pathogenesis of AMD.

All of these findings suggest that complement activation triggers innate immune responses in the subretinal space. The co-distribution of IgG and terminal complement complexes in drusen indicate that immune responses that directly target antigens in retinal cells might also be occurring. Anti-retinal autoantibodies have been reported in a number of ocular disorders, e.g., macular degeneration in an aged monkey model.

2.4. Animal models for AMD

Access to appropriate biological materials from affected donors at different stages of a disease is an absolute necessity for the study of mechanisms underlying the disease process. However, because it is nearly impossible to obtain retinal tissues from patients or controls, the development of animal models becomes crucial for investigating the biological pathways involved in the progression of the disease and for the

development of therapeutic strategies.

Over the past few years, genetic engineering techniques have generated a number of animal models of AMD in mice, rats, rabbits, pigs, and dogs (16). However in mammals, a well-defined fovea is found only in primates (humans and monkeys), and a search for a monkey line affected with macular degeneration has been persistent for a long time.

A monkey with macular degeneration was first described by Stafford et al in 1974. They reported that 6.6 % of the elderly monkeys they examined showed pigmentary disorders and drusen-like spots (17). El-Mofty et al reported that the incidence of maculopathy was 50% in a colony of rhesus monkeys at the Caribbean Primate Research Center of the University of Puerto Rico (18). At the Tsukuba Primate Research Center (Tsukuba City, Japan), Suzuki et al found a single cynomolgus monkey (*Macaca fascicularis*) in 1986 with a large number of small drusen around the macular region (Fig. 4) (19-21). This single affected monkey has multiplied to a large pedigree of more than 65 affect and 210 unaffected monkeys. Drusen were observed in the macular region as early as one year after birth, and the numbers increased and

spread toward the peripheral retina throughout life. No histological abnormalities have been found in the retina, retinal vessels, or choroidal vasculatures of the eyes with drusen. Immunohistochemical and proteomic analyses of the drusen from these monkeys showed that the drusen were very similar to those in other monkeys with aged macular degeneration sporadically found in older monkeys and also with human drusen (22, 23). These observations by Umeda et al have shown that the Tsukuba monkeys produce drusen that are biochemically similar to those in human AMD patients, but the development of the drusen occurs at an accelerated rate of over 25 times. Currently, 240 loci of the cynomolgus monkey are being investigated to try to identify the disease causing gene and to understand the biological pathways leading to complement activation.

The eyes of monkey are structurally similar to human eyes which make them extremely valuable for macular degeneration studies. However, there are limitations in using this species over other laboratory animals. Monkeys have a relatively longer life span, have a longer gestation period, have a lower birth numbers resulting in a slower rate of expanding the pedigree, more difficult to genetically manipulate, and the cost of

maintenance is high. In the other laboratory animals, the differences in the eye structure, lack of a fovea, and a low cone/rod ratio compared to humans have been considered to be a disadvantage for using them as AMD models. However, they are easier to manipulate genetically and easier and less expensive to maintain. This has made the development of a mouse model of AMD very attractive, and a number of mouse AMD models have been reported recently.

The mouse model described by Ambati et al is deficient either in monocyte chemoattractant protein-1 or its cognate C-C chemokine receptor-2. These mice were found to develop the cardinal features of AMD including accumulation of lipofuscin in drusen beneath the RPE, photoreceptor atrophy, and CNV (24). An impairment of macrophage recruitment allowed the accumulation of C5a and IgG, which leads to the production of vascular endothelial growth factor by the RPE cells and the development of CNVs.

Another mouse model that has three known AMD risk factors: age, high fat cholesterol rich diet, and expression of human apolipoprotein E (apoE2, apoE3, apoE4) has been developed (25). ApoE4-deficient mice are severely affected showing diffuse

subretinal pigment epithelial deposits, drusen, thickened Bruch's membrane, and atrophy, hypopigmentation, and hyperpigmentation of the RPE.

Oxidative stress has long been linked to the pathogenesis of AMD. Imamura et al reported a Cu, Zn-superoxide dismutase (SOD1)-deficient mice that had features typical of AMD in human. Senescent Sod1 (-/-) mice had drusen, thickened Bruch's membrane, and choroidal neovascularization (26). The number of drusen increased with age and also after exposure of young Sod1 (-/-) mice to excess light. The retinal pigment epithelial cells of Sod1 (-/-) mice showed oxidative damage, and their beta-catenin-mediated cellular integrity was disrupted. These findings suggested that oxidative stress may affect the junctional proteins necessary for the barrier integrity of the RPE. These observations strongly suggested that oxidative stress may play a major role in AMD.

The complement components, C3a and C5a, are present in drusen, and were observed in Bruch's membrane of a laser-induced CNV mice model. Neutralization of C3a or C5a by antibody or by blockade of their receptors by a complement inhibitor significantly reduced the CNV. These observations revealed a role for immunological